INTERNATIONAL JOURNAL OF
COASTAL & OFFSHORE ENGINEERING
IJCOE Vol.3/No. 3/Autumn 2018 (41-51)

*Available online at: http://ijcoe.org/browse.php?a_code=A-10-184-1&sid=1&slc_lang=en*

# Sensitivity of an Axi-Symmetric Tropical Cyclone Model to Two External Parameters

**Nafiseh Pegahfar [1]*, Maryam Gharaylou [2]**

[1]*Assistant Professor, Atmospheric Research Center, Iranian National Institute for Ocean-ography and Atmospheric Science, Tehran, Iran; pegahfar@inio.ac.ir*
[2]*Assistant Professor, Institute of Geophysics, University of Tehran, Tehran, Iran; gharaylo@ut.ac.ir*

**ARTICLE INFO**

*Article History:*
Received: 18 Oct. 2018
Accepted: 17 Dec. 2018

*Keywords:*
Tropical Cyclone Haiyan
Numerical Model
Convective Entropy Flux
External parameters

**ABSTRACT**

More realistic simulation of hazards caused by Tropical Cyclones (TCs) requires knowledge of the mechanisms that formulate tropical cyclone. Here, sensitivity of an idealized framework has been tested to investigate role of two external parameters in vertical entropy flux. The first parameter controls the ratio of width of eyewall and downdraft regions to radius of maximum wind and the second parameter controls radial decay of wind velocity between two regions. This numerical model used conservation principles, assumed axi-symmetry and steadiness to model TC vortex, and let ventilation be occurred via the path-ways of downdrafts outside eyewall and eddy fluxes directly into eyewall. To test this framework, Tropical Cyclone Haiyan (TCH, formed over the Western part of Pacific Ocean on 3 November 2013) has been selected. Two kinds of datasets including Joint Typhoon Warning Centers (JTWC) Best Track data of Japan Meteorology Agency and Global Forecast System Analysis (GFS-ANL) data have been used. The model has been run for 60 different configurations, based on change of the two external parameters and size of two random do-mains. The sensitivity of the modeled convective entropy flux to the applied changes has been examined via two different aspects of investigation. In the first aspect, terms of the reference equation of convective entropy flux have been considered and their responses to the changes have been studies. While in the second aspect, values of the convective entropy flux at TCH peak activity time (PAT), before and after that have been inspected. Results, obtained from the first aspect, obviously indicate that the increase of the first external parameter increases the all terms of the referred equation, while increase of the second external parameter influenced the terms differently. Also enlarging the domains' size does not impress the results similarly. Outcomes of the second aspect reveal that the implemented changes non-uniformly impact the values of the modeled convective entropy flux in the three considered times.

## 1. Introduction

Since Tropical Cyclone (TC) severe weather are most hazardous in coastal regions and caused extensive damage, loss of life and damaging floods hundreds of miles inland, achieving an entire body of knowledge of hurricane behavior is essential to model hurricane hazard (Vickery et al. 2009; Pielke Jr. et al., 2008). Built up more property along the world's vulnerable coastlines would increase the need of guarantee of TC damage in future. Hence, it is important to understand the physics of TCs in order to improve the ability for short- and long-term forecasts. To understand TC characteristic, various parts of that including inner-core (Montgomery and Smith, 2014; Chen et al. 2018), outer-core (Wang, 2012; Lee et al., 2010; Lin et al. 2017; Schenkel et al. 2018) and TC environment (Jones, 1995; Smith et al., 2000) have been considered. In addition, various physical parameters consist of dynamic and thermodynamic ones have been utilized to hypothesize a mechanism by which TC's intensity is affected. Observations indicated that a TC (I) only develops where significant potential heat flux from sea exists, and (II) decays over land even when plentiful amount of moisture and instability exist.

Environmental wind shear is a challenging factor in TC prediction and is observed to be generally detrimental to tropical cyclogenesis (McBride and Zehr, 1981; Zehr, 1992), and is an important component of empirical genesis indices (DeMaria et al., 2001; Emanuel and Nolan, 2004). Numerical modeling studies showed that sufficiently strong vertical wind shear impedes the development of incipient vortices (Tory et al., 2007; Nolan and Rappin, 2008). However, weak wind shear may aid TC genesis by forcing synoptic-scale ascent, especially in baroclinic environments (Davis and Bosart, 2006; Nolan and McGauley, 2012).

One of indirect effects of wind shear is intrusion of low-equivalent potential temperature air into the inner core of a TC that ventilates the incipient disturbance. Advection of environmental dry flow removes the condensation heat from the vortex and prevents TC deepening by decreasing the efficiency of TC heat engine (Nolan, 2007; Marin et al., 2009). Low-entropy entrance at midlevel is hypothesized as a mechanism by which the environmental vertical wind shear can constrain a TC's intensity. Therefore, entropy and also entropy-dependent parameters have been specially considered in developing of some idealized frameworks assessing TC intensity (Emanuel, 1995). These parameters include air-sea thermodynamic disequilibrium (Emanuel, 1986; Emanuel et al., 2004), entropy deficit (Tang and Camargo, 2014; Bruyere et al., 2012), entropy flux (Bryan and Rutonno, 2009). Thermodynamic disequilibrium between the ocean and the atmosphere derives Carnot engine of mature TC and is a principle factor in definition of potential intensity (Emanuel, 1991). Emanuel et al. (2008) showed that entropy deficit between boundary layer and midlevel should be increased with global warming and affect TC formation and intensification. Frank and Ritchie (2001) and Wong and Chan (2004) investigated ventilation (as vertical entropy flux) of the upper level warm core during TC lifetime and Riehl (1951) and Kleinschmidt (1951) studied surface and convective entropy fluxes from ocean during a TC intensification. Results of investigations led to use of entropy as an important parameter in various hypothesis describing both dynamical and thermodynamical mechanisms in TC formation and intensification. Tang and Emanuel (2010) developed a theoretical framework to assess how entropy flux affects TC intensity via two possible pathways (low-level pathway and mid-level pathway). They evaluated that framework for ventilation and potential intensity with fixed values of external parameters.

In this research, the mentioned theoretical concept (with a private source code) has been utilized and the related code has been written by the authors to examine dependency of the convective entropy flux on various values of two external parameters. Following, the theoretical framework (Sec. 2), data and methods (Sec. 3), results and discussion (Sec. 4), summary and conclusions (Sec.5) are presented.

## 2. Theoretical Framework

The source code for this framework is not in the public domain, so we had to develop this algorithm independently. The applied model is based on conservation principles and closely parallels that of Bister and Emanuel (1998). Throughout the derivation, axisymmetry, steadiness and slantwise neutrality (requiring that saturation isentropes be congruent to angular momentum surfaces) are assumed to model TC vortex.

Pseudo-adiabatic entropy has been calculated using the relation defined by Bryan (2008) as:

$$s = \left(c_{pd} + c_l r_v\right)\ln(T/T_R) - R_d \ln(p_d/p_0) + \frac{L_{v0} r_v}{T} - R_v r_v \ln(H) \qquad (1)$$
$$p_d = p - e, \quad e = (r_v * p)/(0.622 + r_v),$$

where the constants of $c_{pd} = 1005$ J/(kgK), $c_l = 4218$ J/(kgK) and $L_{v0} = 2.55 \times 10^{-6}$J/kg are the specific heat at constant pressure for dry air, specific heat for liquid water and latent heat, respectively. The gas constants for water vapor and dry air have been included as $R_v = 461.51$ J/(kgK) and $R_d = 287.05$ J/(kgK), and the constants of $T_R = 273.15$ K and $p_R = 1000$ hPa denote the freezing point of water and reference pressure, in that order. Also the variables of $T$, $p_d$, $H$, $e$, $p$ and $r_v$ demonstrate the temperature, partial pressure for dry air, humidity, water vapor pressure, pressure and water vapor mixing ratio, correspondingly.

The first law of thermodynamics for saturated conditions is combined with the momentum equations and a pseudo-adiabatic assumption, ignoring the contribution of liquid water and ice to the entropy ($s$) is used. It is worthwhile to be noted that unbalanced effects are not absolutely critical to describe the basic behavior of the intensity of ventilation-modified TC. Then the equations are integrated around a closed circuit bounded by two isotherms (Fig. 1a). To achieve the neutrality constrain, the sub-cloud layer is divided up in to two regions, as sketched in Fig. 1b including an "inner" region from $r_1$ to $r_2$ centered around the radius of maximum wind and an "outer" region from $r_2$ to $r_3$. Sources of entropy in both regions include turbulent fluxes ($F_s$), dissipative heating (H), and fluxes by the mean secondary circulation (lateral fluxes). The convective entropy flux, $F_s(z = h) = \overline{\acute{w}\acute{s}}$, through the top of the sub-cloud layer is included in the outer region. Convective downdrafts, in particular, driven by evaporation of rain into the sub-saturated air, are supplied by eddy entropy fluxes in the free troposphere, u′s′, as will be explained later. In a steady state, the entropy flux by

the mean transverse circulation through the boundaries of the sub-cloud layer of the control volume is adequate to the sum of internal sources and sinks of entropy. Then, entropy is assumed constant with height in the sub-cloud layer. The aerodynamic flux formula for the surface flux of entropy is

$$F_s(z=0) = -C_k|u|\,(s^*_{SST} - s_b), \tag{2}$$

where $C_k$ is the enthalpy coefficient, $u$ is wind velocity at surface, $s^*_{SST}$ is the saturation entropy at the sea surface and $s_b$ is the sub-cloud layer entropy. To show the contribution of dissipative heating to the entropy equation, the expression of

$$\int_0^h H dz = \frac{C_D}{T_s}|\mathbf{u}|^3 \tag{3}$$

introduced by Bister and Emanuel (1998), has been used (where the constant of $C_D$ is the drag coefficient and $T_s$ is the surface temperature). To apply the needed approximations, u is expressed as some fraction of the maximum wind velocity,$u_m$, and r (radial distance of u from TC center) is showed as some proportion of the radius of the maximum wind, $r_m$, both in the following fashions of

$$u = \begin{cases} u_m & r_1 < r < r_2 \\ \gamma u_m & r_2 < r < r_3 \end{cases}, \quad r = \begin{cases} r_m & r_1 < r < r_2 \\ \alpha r_m & r_2 < r < r_3 \end{cases} \tag{4}$$

Here, $\gamma$ controls the radial decay of wind and $\alpha$ controls the ratio of the width of both the inner and outer regions to the radius of maximum wind (Fig. 1b). By assuming (I) the turbulent flux of angular momentum at the surface as the aerodynamic flux formula of

$$F_M(z=0) = -C_D|u|r\,v, \tag{5}$$

where v is the azimuthal velocity, and (II) an expression for $< u >$ in the outer-region as

$$< u > \approx -\frac{C_D|u_m|r_m}{h}, \tag{6}$$

the relation of convective entropy flux is obtained as

$$\overline{\acute{w}\acute{s}} = \frac{C_D\gamma|u_m|\alpha}{\alpha - 1}(s_b^o - s_b^i) + C_k\gamma|u_m|(s^*_{SST} - s_a) + \frac{C_D}{T_s}\gamma^3|u_m|^3 \tag{7}$$

where $\overline{\acute{w}\acute{s}}$ is the convective entropy flux, $s_a$ is an ambient value of saturation moist entropy, $s_b^i$ is the sub-cloud layer entropy of the inner region, and $s_b^o$ is the sub-cloud layer entropy of the outer region at $r_3$. The "upwind" like approximation where $s_b^o = s_a$ can be used.

Tang (2010) assumed equal width for both regions ($\alpha = 1$) to simplify the analysis and allocated a value to $\alpha$ that roughly showed the characteristic width of a TC's eyewall. It is worthwhile to note that increase of $\alpha$ increases the radial intrusion of dry air to sub-cloud layer and also allows more surface flux be included. In greater value of $\gamma$ these effects offset another one and $\alpha$ variation leads to ventilation change. Also $\gamma$ value controls the recovery of the downdrafts. Tang and Emanuel (2010) used $0 < \alpha < 3$ and $0.3 < \gamma < 1$ and reported inertially unstable combinations for ventilation and reached a single curve that was invariant across all thermodynamic states. Tang and Emanuel (2010) stated that evaluation of this curve in the nature needs high density time and space at midlevel that is out of the abilities of this research and introduced numerical simulations of ventilated TC as a tool to test this sensible approach.

In the present work, effects of various external parameters have been examined for entropy and its vertical flux during a selected TC.

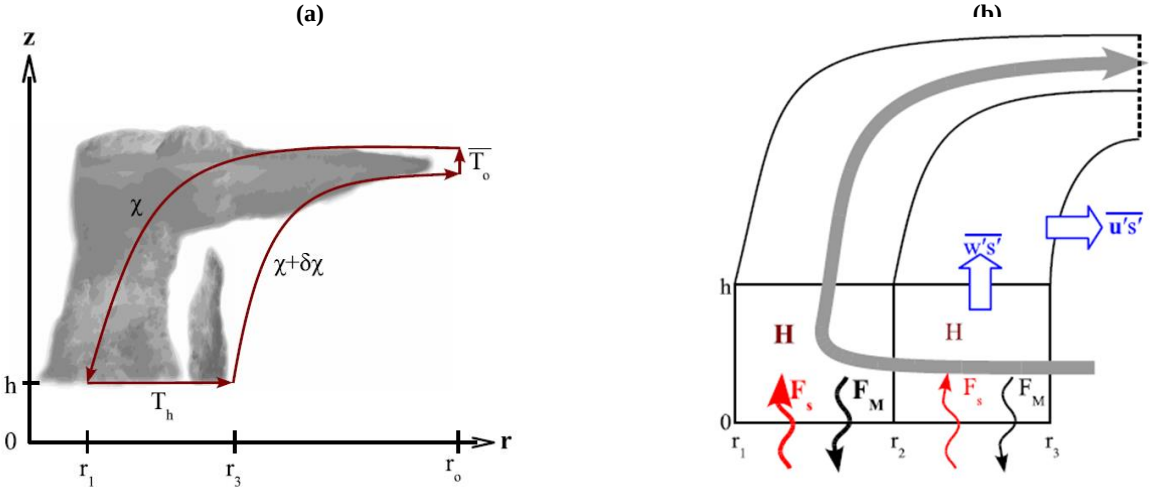


**Figure 1 (a) Closed circuit around which entropy is evaluated. Circuit consists of two isotherms, temperature at cloud base height ($T_h$) and temperature at tropopause height ($T_o$), and two contours of constant $\chi$, where $\chi \in$ {saturated entropy (s∗), momentum (M), mass stream function(ψ)}. (b) Sources and sinks of entropy and angular momentum in the sub-cloud layer and free troposphere for the low-level pathway: surface fluxes of entropy, $F_s(z=0)$, and angular momentum, $F_M(z=0)$ (wavy arrows); dissipative heating, H; advection by the secondary circulation (gray arrow); convective entropy flux, $\overline{\acute{w}\acute{s}}$ (vertical block arrow); and eddy entropy flux, $\acute{u}\acute{s}$, through outer angular momentum surface in the free troposphere (horizontal block arrow) (from Tang, 2010)**

## 3. Data and methods

In the present work, two datasets have been used. The first dataset was from Joint Typhoon Warning Centers (JTWC) Best Track data of Japan Meteorology Agency and included eye location (latitude and longitude), maximum wind speed and its radius. The second dataset was taken from NCEP-GFS analysis data with $0.5^o \times 0.5^o$ horizontal resolution at 26 pressure levels with 6-h intervals. Temperature, humidity, pressure and mixing ratios data at various level heights have been extracted from NCEP-GFS analysis data to calculate entropy and its derivatives at surface, cloud base height and also through boundary layer. All data have been used during 3-11 November 2013. Entropy and its convective flux, have been computed at each grid points of all considered domains that will be described later. To this aim, we computed all values via our NCL (NCAR Command Language) scripts.

To assess dependency of the applied framework on (I) the size of the inner- and outer regions ($\alpha$) and also (II) the radius of decay of wind velocity from inner to outer regions ($\gamma$), 60 experiments have been run. List of $\alpha$ and $\gamma$ values have been shown in Table 1 for 60 experiments. In these experiments, the value of α varies from 1.2 to 3 (including 1.25, 1.3, 1.4, 1.5, 1.67, 1.75, 2, 2.3 and 3) and the γ value ranges from 0.3 to 0.9 (0.3, 0.5, 0.8 and 0.9). For this purpose, the size of the inner region differs from $1^o \times 1^o$ to $5^o \times 5^o$, while the size of the outer region changes from $2^o \times 2^o$ to $7^o \times 7^o$. It should be noted that these regions are different from TC inner- and outer-core, and have been defined randomly.

**Table 1 list of $\alpha$ and $\gamma$ values**

| Num. | size of the inner region ($x^\circ \times x^\circ$) | size of the outer region ($x^\circ \times x^\circ$) | calculated $\alpha$ | $\gamma$ |
|---|---|---|---|---|
| 1 | 1 | 2 | 2 | 0.3, 0.5, 0.8 and 0.9 |
| 2 | 1 | 3 | 3 | 0.3, 0.5, 0.8 and 0.9 |
| 3 | 2 | 3 | 1.5 | 0.3, 0.5, 0.8 and 0.9 |
| 4 | 2 | 4 | 2 | 0.3, 0.5, 0.8 and 0.9 |
| 5 | 2 | 5 | 2.5 | 0.3, 0.5, 0.8 and 0.9 |
| 6 | 2 | 6 | 3 | 0.3, 0.5, 0.8 and 0.9 |
| 7 | 3 | 4 | 1.33 | 0.3, 0.5, 0.8 and 0.9 |
| 8 | 3 | 5 | 1.67 | 0.3, 0.5, 0.8 and 0.9 |
| 9 | 3 | 6 | 2 | 0.3, 0.5, 0.8 and 0.9 |
| 10 | 3 | 7 | 2.33 | 0.3, 0.5, 0.8 and 0.9 |
| 11 | 4 | 5 | 1.25 | 0.3, 0.5, 0.8 and 0.9 |
| 12 | 4 | 6 | 1.5 | 0.3, 0.5, 0.8 and 0.9 |
| 13 | 4 | 7 | 1.75 | 0.3, 0.5, 0.8 and 0.9 |
| 14 | 5 | 6 | 1.2 | 0.3, 0.5, 0.8 and 0.9 |
| 15 | 5 | 7 | 1.4 | 0.3, 0.5, 0.8 and 0.9 |

Tropical cyclone Haiyan (TCH) with the extra-ordinary intensity of 170 kts (at 1800 UTC 7 November) intensified as the highest ever observed TCs globally and reached 35 kts well above the threshold of 135 kts as the existing highest value for category-5 (Lin et al., 2014). TCH devastated the southeast part of Asia, especially the Philippines Islands, and killed 6300 persons. TCH formed at 6°53′N/158°14′E on 2 November 2013, become a tropical storm on 4 November 2013, and reached the intensity of a typhoon on 5 November, based on saffir-simpson hurricane wind scale. TCH reached the maximum intensity at 12:00 UTC 7 November 2013, and after that entered the Philippines Islands. TCH continued northwesterly motion to the northern part of the Vietnam and dissipated on 11 November 2013. Some dynamic, thermodynamic and synoptic features of TCH have been studied by Pegahfar and Ghafarian (2017, 2104). Moreover, some of the upper and lower tropospheric meteorological parameters have been considered during TCH by Pegahfar and Ghafarian (2016). Shimada et al. (2018) examined the structure of TCH inner core. Wang et al. (2018) investigated the role of warm-core ocean eddy on TCH rapid intensification.

## 4. Results and discussion

To assess dependency of the applied framework on the size of the inner- and outer regions and also the radius of the maximum wind speed, 60 experiments have been run. Time series of (I) discrepancy of entropy between the inner- and outer regions, (II) three right terms of Eq. 7 and (III) $\overline{\acute{w}\acute{s}}$ values have been calculated for all experiments and analyzed. As an example, the results of two experiments have been plotted in Fig. 2. The inner regions of $1^o \times 1^o$ and $3^o \times 3^o$, the outer regions of $2^o \times 2^o$ and $6^o \times 6^o$, with $\gamma = 0.9$ have been plotted in Figure 2I and 2II, respectively.

In this figure, the time series of discrepancy of entropy between the inner- and outer regions ("a" panels in Fig. 2I and 2II), three right terms of Eq. 7 ("b", "c" and "d" panels in Fig. 2I and 2II) together with values of $\overline{\acute{w}\acute{s}}$ ("e" panels in Fig. 2I and 2II) have been presented. It can be realized that the first term has negative effect on $\overline{\acute{w}\acute{s}}$, while the second and third terms play positive influence. A remarkable point of Fig. 2 is the existence of two relative maximum values of $\overline{\acute{w}\acute{s}}$, one before 1800 UTC 07 November (TCH peak activity time, hereafter, TCHPAT) and the other after TCHPAT. Figure 2 indicates that the relatively maximum value of $\overline{\acute{w}\acute{s}}$ after TCHPAT did not occur at the same time using various experiments.

To analyze the results of all experiments, Figs. 3-5 have been prepared to demonstrate the minimum values of the first right-hand side term of Eq. 7 and maximum values of the second and third terms according to various $\alpha$ values in logarithmic scale, correspondingly. In Figs. 3-5, the results of selecting $\gamma = 0.9, 0.5$ and $0.3$ have been presented and each marker has been labeled by the size of the inner domain side.

(I)

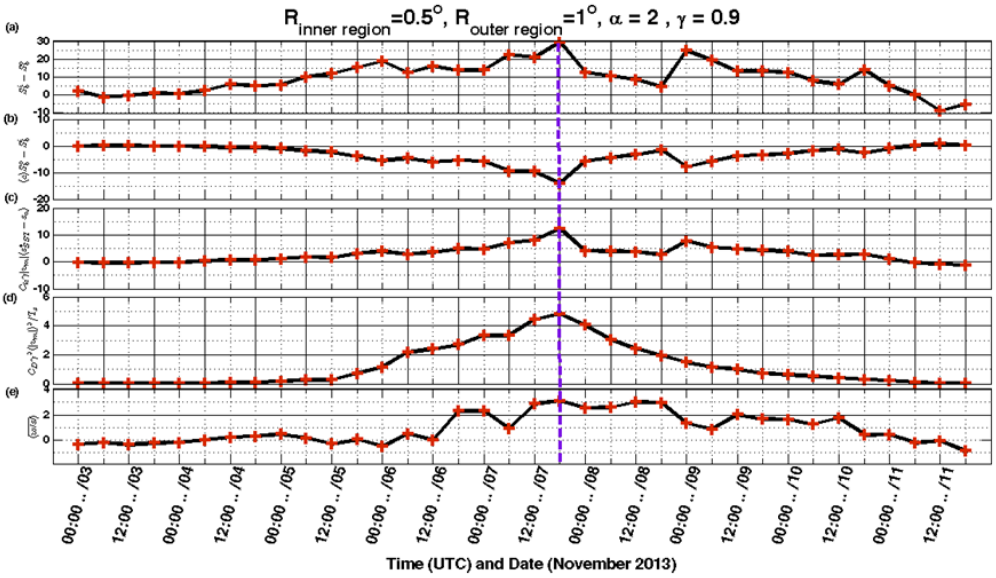


(II)

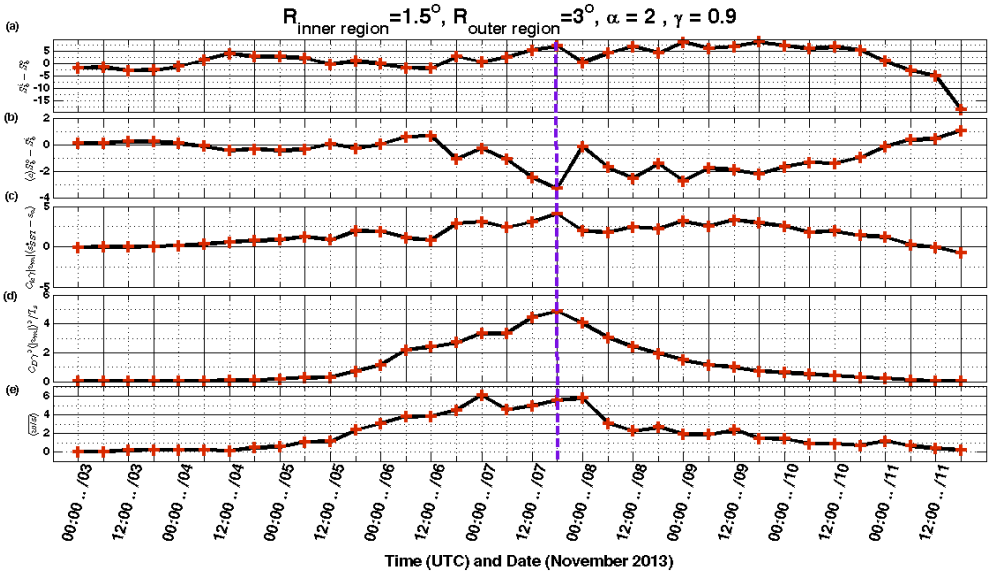


**Figure 2 Time series of discrepancy between entropy in inner and outer regions ($s_b^o - s_b^i$, (J/(kg K))) (a), three right terms of Eq. 7 (b, c, d) and also $\overline{w's'}$ (W/(K m$^2$))(d). The selected case include $1^o \times 1^o$ inner region, $2^o \times 2^o$ outer region (I subplot) and $3^o \times 3^o$ inner region, $6^o \times 6^o$ outer region (II subplot), both for $\gamma = 0.9$. The sign of "R" shows the radius of the regions. Inner- and outer regions have been demonstrated as subscribes of "R" signs.**

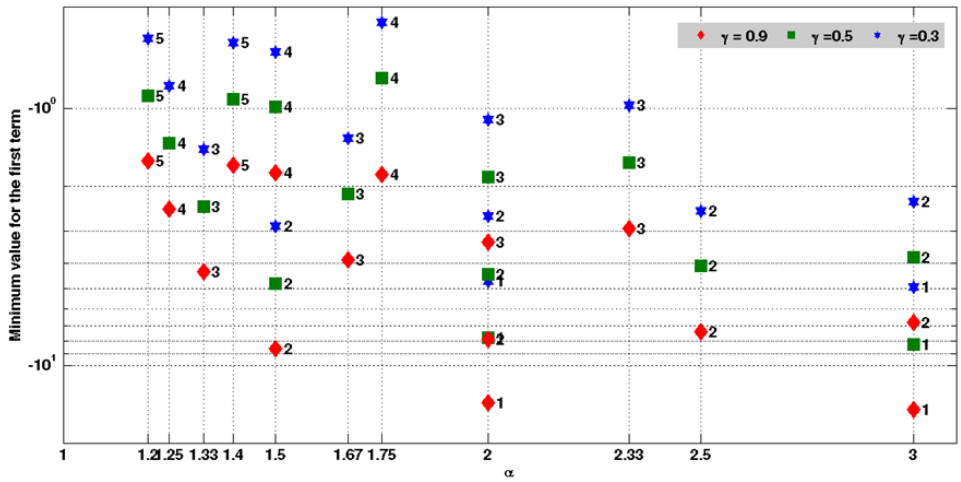


**Figure 3 Distribution of the minimum values of the first right-hand side term (W/(K m$^2$)) of Eq.7, according to the various values of α and γ, and different size for the inner and outer domains. The size of the inner domain side has been added to the right of each marker.**

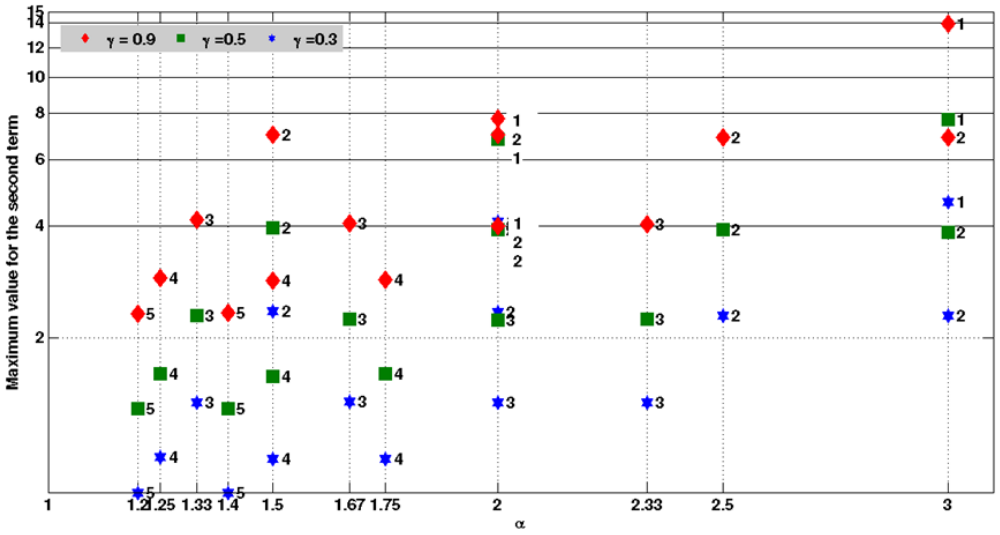


**Figure 4 Same as Fig. 3 but for the maximum values of the second right-hand side term ($W/(K\,m^2)$ ) of Eq.7.**

Figure 3 shows that the smaller inner regions produce the smaller values, and enlarging the inner region size decreases the role of the first term of Eq.7. Also greater γ values lead to larger extreme values of the first term of Eq.7.

Figure 4 demonstrates that increase of γ and α values increase the maximum value of the second term, while increase of the inner region size decreases the corresponding maximum value. It can be realized from Fig. 5 that only increase of γ value increases the maximum value of the third term, while increase of α value and inner region size has no effect. Here after results from the experiments with $\gamma = 0.9$ and $\gamma = 0.8$ will be presented, because of producing the largest absolute values.

As it can be seen from Fig. 2, time series of $\overline{\acute{w}\acute{s}}$ has two relative maximum values, before and after TCHPAT, respectively. For a comprehensive analysis, variation of these two values align with the value at the TCHPAT have been studied using various γ and α values. An overview of $\overline{\acute{w}\acute{s}}$ time series through 60 experiments indicates that the first relative maximum value of $\overline{\acute{w}\acute{s}}$ before TCHPAT occurred between 1800 UTC 6 November and 0000 UTC 7 November, while its second relative maximum value after TCHPAT happened between 0000 and 1200 UTC 8 November. The calculated values of $\overline{\acute{w}\acute{s}}$ for the first relative maximum value before and after TCHPAT together with the values at TCHPAT have been presented in Fig. 6. As this figure demonstrates, choosing $\gamma = 0.9$ and $\gamma = 0.8$ values produces close values of $\overline{\acute{w}\acute{s}}$ especially for the two relative maximum ones, however the first choice of $\gamma$ creates higher values. Changing $\alpha$ and $\gamma$ values leads to significant variation in $\overline{\acute{w}\acute{s}}$ value at TCHPAT and also for two relative maximum values. Also increase of the outer region sizes in experiments with the same inner region sizes rises the values of $\overline{\acute{w}\acute{s}}$.

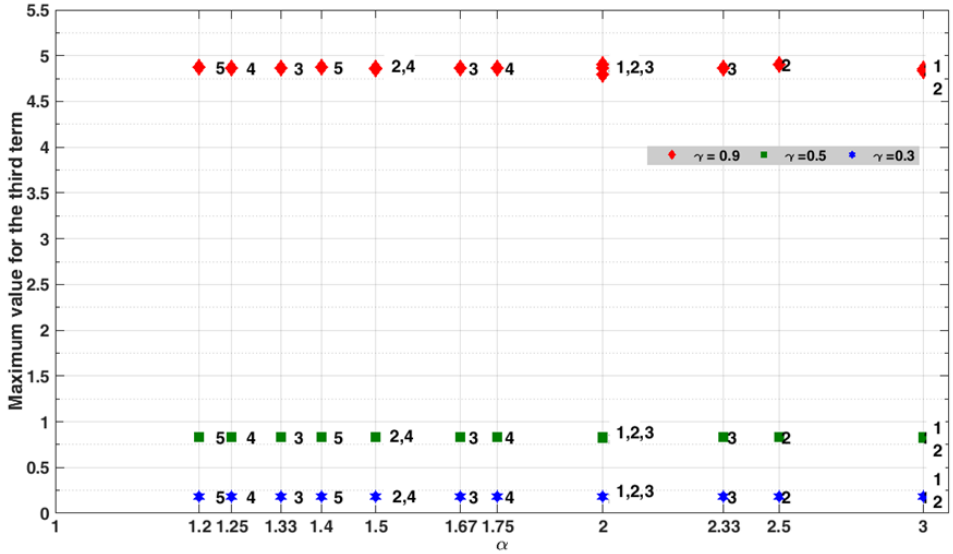


**Figure 5 Same as Fig. 3 but for the maximum values of the third right-hand side term ($W/(K\,m^2)$) of Eq.7.**

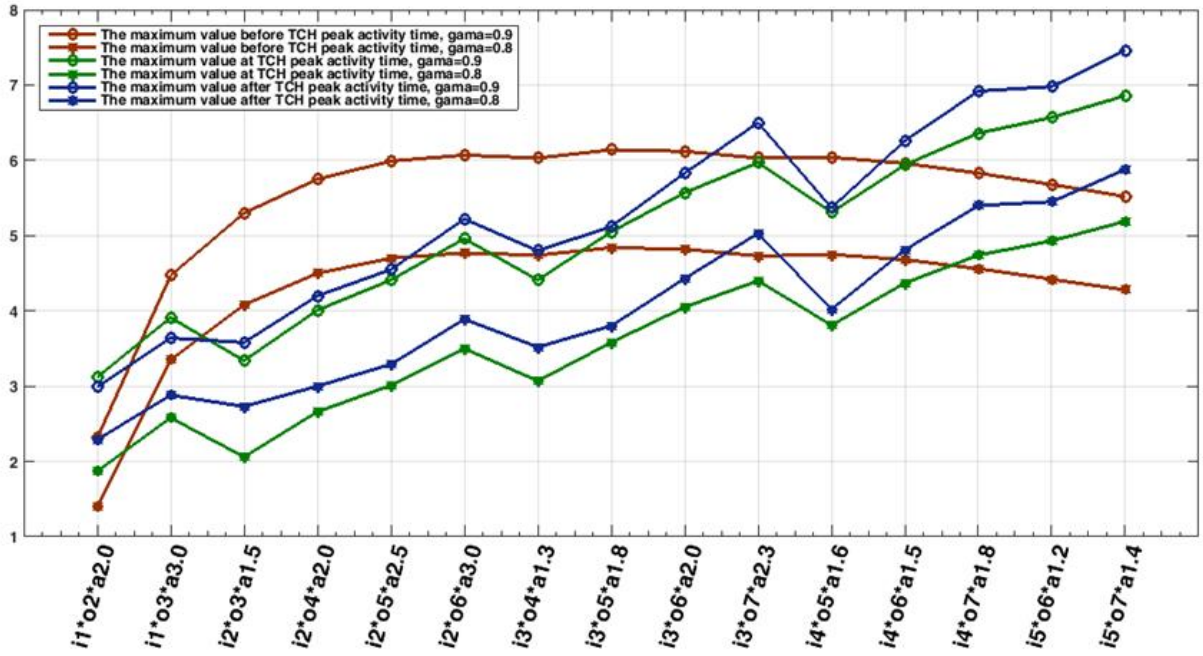


**Figure 6 the value of $\overline{\acute{w}\acute{s}}$ ($\mathrm{W}/(\mathrm{K\,m^2})$) at TCHPAT align with two relative maximum values of $\overline{\acute{w}\acute{s}}$ before and after TCHPAT, respectively. X-abscissa is labeled as "im*on*ap", where "im" denotes the size of inner region side, "on" shows the size of outer region side and "ap" is the α and its value. Values obtained using $\gamma = 0.9$ are denoted by circle and those from $\gamma = 0.8$ are signified by asterisks.**

Moreover, increase of the inner region sizes in the experiments with the same outer region sizes growths the values of $\overline{\acute{w}\acute{s}}$. Increase of $\alpha$ values, without any attention to the inner- and outer region sizes, leads to higher values of $\overline{\acute{w}\acute{s}}$. The first relative maximum value of $\overline{\acute{w}\acute{s}}$ shows relatively constant behavior for the inner domains larger than $2° \times 2°$ and the outer domains greater than $4° \times 4°$, while its value is sensitive to the inner domains smaller than $2° \times 2°$ and the outer domains smaller than $4° \times 4°$.

Variation of the two relative maximum values of $\overline{\acute{w}\acute{s}}$ (before and after TCHPAT) and the value at TCHPAT have been plotted in Fig. 7, based on the various inner – and outer domain sizes. Value of each bar has been added to the top of that. As before, two values of $\gamma = 0.9$ and $\gamma = 0.8$ have been plotted in this figure. As Fig. 7 shows, the inner regions greater than $1° \times 1°$ produce little variation in the first relative maximum value of $\overline{\acute{w}\acute{s}}$, around 5-6 for $\gamma = 0.9$ and 4 for $\gamma = 0.8$, while the experiments with inner region of $1° \times 1°$ lead to the smaller values at both values of $\gamma$.

To analysis dependency of the three special times in $\overline{\acute{w}\acute{s}}$ time series (before, after and at TCHPAT) on the inner and outer domain sizes and also on $\alpha$ and $\gamma$ values separately, Figs. 8-10 have been prepared.

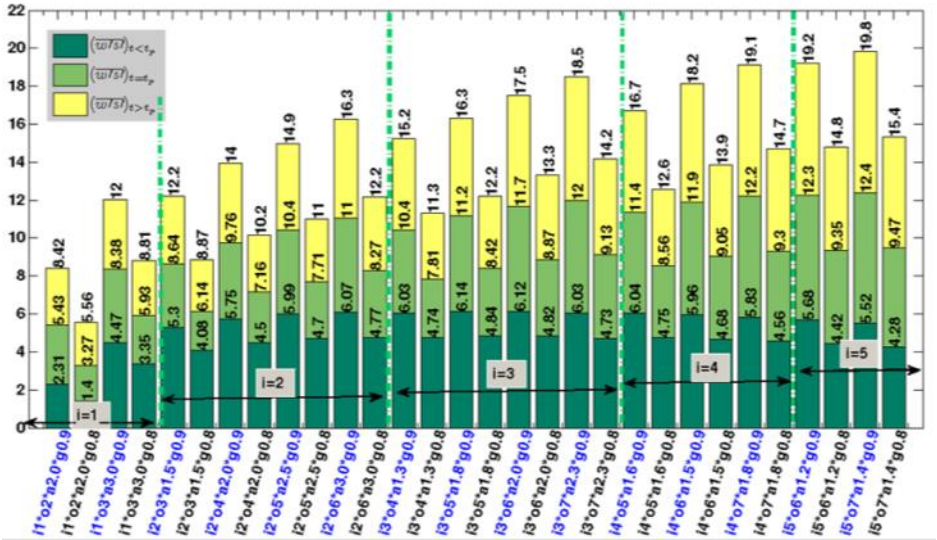


**Figure 7 the value of $\overline{\acute{w}\acute{s}}$ ($\mathrm{W}/(\mathrm{K\,m^2})$) is dark green before TCHPAT ($t < t_p$), light green at TCHPAT ($t_p$) and yellow after TCHPAT ($t > t_p$). The X- abscissa is labeled as "im*on*ap*gt", where "im" denotes the size of inner region side, "on" shows the size of outer region side, "ap" is the α and its value and "gt" refers $\gamma$ and its value.**

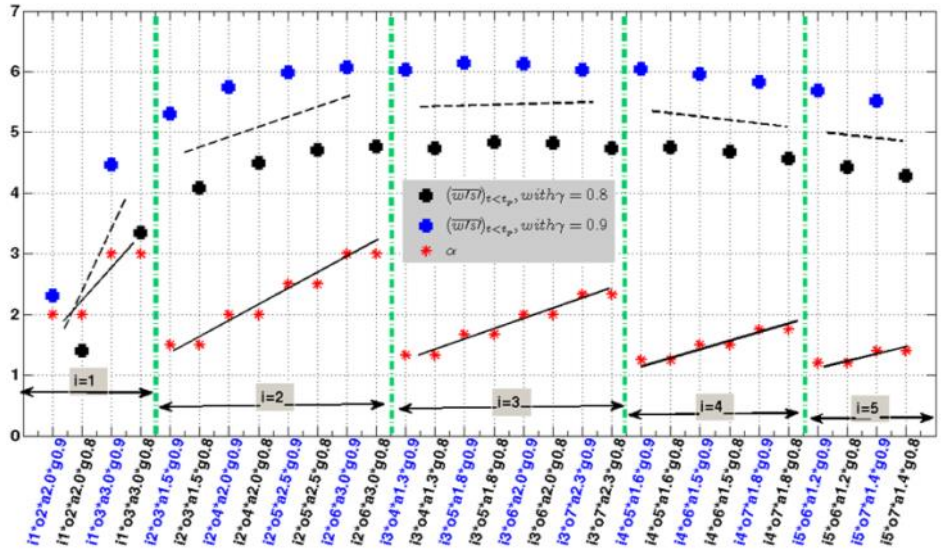


**Figure 8 values of $\overline{\acute{w}\acute{s}}$ ($\mathbf{W/(K\,m^2)}$) before TCHPAT ($t < t_p$, dark green) for two values of $\gamma = 0.9$ (blue plus) and $\gamma = 0.8$ (black plus). The X- abscissa is labeled as "im*on*ap*gt", where "im" denotes the size of inner region side, "on" shows the size of the outer region side, "ap" is the α and its value and "gt" shows the $\gamma$ and its value.**

Figure 8 shows relative maximum value of $\overline{\acute{w}\acute{s}}$ before TCHPAT for the experiments with $\gamma = 0.9$ and 0.8 and various inner- and outer domain sizes. Independency of the value of the first relative maximum value of $\overline{\acute{w}\acute{s}}$ on the inner- and outer domain sizes for the experiments with the inner domain greater than $2° \times 2°$ is evident. Changing inner domain size from $1° \times 1°$ to $2° \times 2°$ increases the first maximum value of $\overline{\acute{w}\acute{s}}$ significantly.

Figure 9 demonstrates that at TCHPAT, in the experiments with the same inner domain size and different outer domain size (various $\alpha$), increase of $\alpha$ value leads to greater value of $\overline{\acute{w}\acute{s}}$. In the experiments with the same value of $\alpha$, the larger inner domain produce larger $\overline{\acute{w}\acute{s}}$ values. The value of $\overline{\acute{w}\acute{s}}$ at TCHPAT is dependent on inner- and outer domain size and also $\alpha$ and $\gamma$ values. At TCHPAT, the smallest value of $\overline{\acute{w}\acute{s}}$ belongs to the experiments with smaller inner domain size ($i = 1$). Results from Figs 9 and 10 are similar.

## 5. Summary and conclusions

Forecasting the activity of severe TCs as significant natural hazards along with improving understand of their plausible impacts are an important task (Camargo et al. 2007). In the present work, a theoretical framework developed by Tang (2010) has been utilized. The source code of this axi-symmetric framework was not freely available and the authors developed that independently. There were two external parameters in this model that controlled the results. One of them was $\alpha$ parameter that shows the ratio of the outer domain size to the inner one. The other one was $\gamma$ parameter that expressed the wind

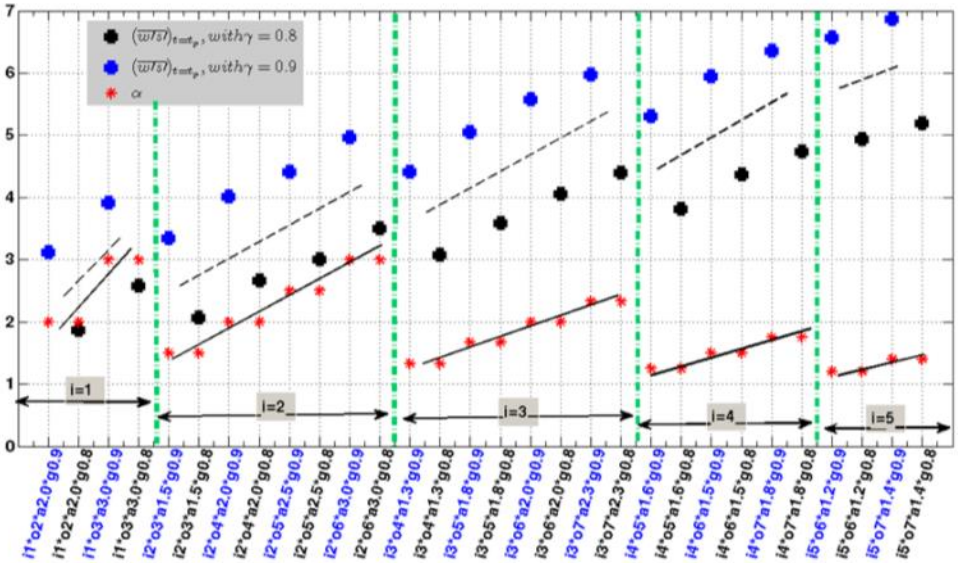


**Figure 9 values of $\overline{\acute{w}\acute{s}}$ ($\mathbf{W/(K\,m^2)}$) at TCHPAT ($t = t_p$, dark green) for two values of $\gamma = 0.9$ (blue plus) and $\gamma = 0.8$ (black plus). The X-abscissa is labeled as "im*on*ap*gt", where "im" denotes the size of inner region side, "on" shows the size of the outer region side, "ap" is the α and its value and "gt" shows the $\gamma$ and its value.**

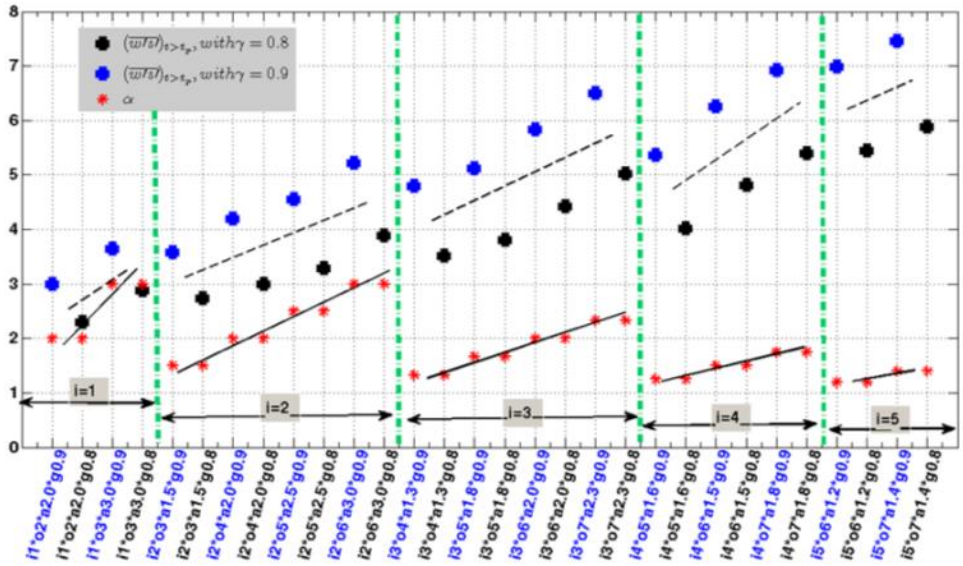


**Figure 10 values of $\overline{\dot{w}\dot{s}}$ ($\mathbf{W/(K\,m^2)}$) after the TCHPAT ($t > t_p$, dark green) for two values of $\gamma = 0.9$ (blue plus) and $\gamma = 0.8$ (black plus). The X- abscissa is labeled as "im*on*ap*gt", where "im" denotes the size of inner region side, "on" shows the size of outer region side, "ap" is the α and its value and "gt" shows the $\gamma$ and its value.**

speed as a fraction of maximum wind speed. To investigate the sensitivity of this model to these parameters, it was run for 60 different configurations. Various configurations were set using different $\alpha$ and $\gamma$ values and also inner- and outer domain sizes. The α value varied from 1.2 to 3 and γ value ranged from 0.3 to 0.9. Also the inner region size differed from $1^o \times 1^o$ to $5^o \times 5^o$, while the outer region changed from $2^o \times 2^o$ to $7^o \times 7^o$. Values of $\overline{\dot{w}\dot{s}}$ were calculated using Eq. 7 including three main terms.

The outputs were analyzed from the two different aspects categories as (I) three right-hand side terms of the applied main equation (Eq. 7) and (II) importance of two relative maximum values of $\overline{\dot{w}\dot{s}}$ before and after TCHPAT and also $\overline{\dot{w}\dot{s}}$ value at TCHPAT.

Investigation of the first aspect showed that the increasing of $\gamma$ value increased the importance of all terms. In addition, increase of the specific volume (α) led to the increase of the contributions of entropy discrepancy between the inner and outer regions at both cloud base height and surface (the first and second right-hand-side terms), while it had no effect on the maximum wind speed (the third right-hand-side term).

Analysis of two maximum values of the convective entropy flux before and after TCHPAT and that at the TCHPAT revealed that the effects of variation of $\alpha$ and $\gamma$ values and also change of the inner- and outer domain sizes at these three considered times were not the same. The inner domain size smaller than $2° \times 2°$ and the outer domain size smaller than $4° \times 4°$ produced noticeable variations for the corresponding values before TCHPAT, while the larger inner- and outer domain sizes didn't affect the results importantly. Values of vertical entropy flux at TCHPAT and also its maximum value after TCHPAT are sensitive to $\alpha$ and $\gamma$ values and also the inner- and outer domain sizes. A thorough evaluation showed that both enlarge of the inner domain size along with the constant outer domain size, and extend of the outer domain size with constant inner domain size led to the increase of the convective entropy flux.

Overall, findings of this research showed that configuration of the model (including the two external parameters and domains' size) affected the convective entropy flux outputs during the TCH from two different aspects. Since a TC experiences various extensions and intensities during its lifetime, reaching a comprehensive conclusion to define an optimized configuration needs data with higher horizontal grid resolution and also more TCs for test. The authors are implementing this subject based on downscaling approach.

## Acknowledgement

This work was funded by the Iranian National Institute for Oceanography and Atmospheric Science (project No. 393-033-02). The authors would like to thank NCEP-GFS teams for providing analysis data and also JTWC for TCH track data.

## 6. References

1- Bister, M., & Emanuel, K., (1998), *Dissipative heating and hurricane intensity*, Meteorology Atmospheric Physics, 65, 233–240.

2- Bruyère, C. L., Holland, G. J., & Towler, E., (2012), *investigating the use of a genesis potential index for tropical cyclones in the North Atlantic basin*, Journal of Climate, 2524, 8611-8626.

3- Bryan, G. H., (2008), *On the computation of pseudoadiabatic entropy and equivalent potential temperature*, Mon. Wea. Rev., 13612:5239-5245.

4- Bryan, G., & Rotunno, R., (2009), *The maximum intensity of tropical cyclones in axisymmetric numerical model simulations*, Mon. Wea. Rev., 137, 1770–1789.
5- Camargo, S. J., A. H. Sobel, A. G. Barnston, and K. A. Emanuel, (2007b), *Tropical cyclone genesis potential index in climate models*. Tellus, 59A, 428–443.
6- Davis, C., & Bosart, L., (2006), *The formation of Hurricane Humberto 2001: The importance of extratropical precursors*, Quart. J. Roy. Meteor. Soc., 132, 2055–2085.
7- DeMaria, M., Knaff, J., & Connell, B., (2001*), A tropical cyclone genesis parameter for the tropical Atlantic*, Wea. Forecasting, 16, 219–233.
8- Chen, X., Wang, Y., Fang, J., & Xue, M., (2018), *A Numerical Study on Rapid Intensification of Typhoon Vicente (2012) in the South China Sea. Part II: Roles of Inner-Core Processes*, Journal of the Atmospheric Sciences, 75(1), 235-255.
9- Emanuel, K. A., (1986), *An air–sea interaction theory for tropical cyclones. Part I: Steadystate maintenance*, J. Atmos. Sci., 43, 585–604.
10- Emanuel, K. A., (1991), *The theory of hurricanes*, Annual Review of Fluid Mechanics, 231, 179-196.
11- Emanuel, K. A., (1995), *Sensitivity of tropical cyclones to surface exchange coefficients and a revised steady-state model incorporating eye dynamics*, J. Atmos. Sci., 52, 3969– 3976.
12- Emanuel, K., & Nolan, V., (2004), *Tropical cyclone activity and the global climate system. Preprints*, 26th Conf. on Hurricanes and Tropical Meteorology, Miami, FL, Amer. Meteor. Soc., 240–241.
13- Emanuel, K., DesAutels, C., Holloway, C., & Korty, R., (2004), *Environmental control of tropical cyclone intensity*, J. Atmos. Sci., 617, 843-858.
14- Emanuel, K., Sundararajan R., & Williams J., (2008), *Hurricanes and global warming - results from downscaling IPCC AR4 simulations*, Bull. Amer. Meteor. Soc., 89, 347–367.
15- Frank, W. M., & Ritchie, E. A., (2001), *Effects of vertical wind shear on the intensity and structure of numerically simulated hurricanes*, Mon. Wea. Rev., 129, 2249–2269.
16- Jones, S., (1995), *The evolution of vortices in vertical shear. I: Initially barotropic vortices*, Quart. J. Roy. Meteor. Soc., 121, 821–851.
17- Kleinschmidt E., (1951), *Grundlagen einer theorie der tropischen zyklonen*, Arch. Meteor. Geophys. Bioklimatol., 4A, 53–72.
18- Lee, C. S., Cheung, K. K., W., Fang, W. T., Elsberry, R. L., (2010), *Initial maintainance of tropical cyclone size in the western North Pacific*, Mon. Wea. Rev., 138(8), 3207-3223.
19- Lin, I. I., Pun, I. F., & Lien, C. C., (2014), *"Category-6" supertyphoon Haiyan in global warming hiatus: Contribution from subsurface ocean warming*, Geophysical Research Letters, 41(23), 8547-8553.
20- Lin, N., Jing, R., Wang, Y., Yonekura, E., Fan, J., & Xue, L. (2017), *A statistical investigation of the dependence of tropical cyclone intensity change on the surrounding environment*, Mon. Wea. Rev., 145, 2813–2831
21- Marin, J., Raymond, D., & Raga, G., (2009), *Intensification of tropical cyclones in the GFS model*, Atmos. Chem. Phys., 9, 1407–1417.
22- McBride, J., & Zehr, R., (1981), *Observational analysis of tropical cyclone formation. Part II: Comparison of non-developing versus developing systems*, J. Atmos. Sci., 38, 1132–1151.
23- Montgomery, M. T., & Smith, RK., (2014), *Paradigms for tropical cyclone intensification*, naval postgraduate school Monterey ca dept. of meteorology.
24- Nolan, D., & Rappin, E., (2008), *Increased sensitivity of tropical cyclogenesis to wind shear in higher SST environments*, Geophys. Res. Lett., 35, L14805, doi: 10.1029/2008GL034147.
25- Nolan, D., & McGauley, M., (2012), *Tropical cyclogenesis in wind shear: Climatological relationships and physical processes*, Cyclones: Formation, Triggers, and Control, 1-36.
26- Nolan, D., (2007), *What is the trigger for tropical cyclogenesis?*, Aust. Meteor. Mag., 56, 241–266.
27- Pegahfar, N., & Ghafarian, P., (2014), *Analysis of two dynamic parameters of CAPE and Helicity for Haiyan Tropical Cyclone*, International ICOPMAS Conference, Tehran, Iran.
28- Pegahfar, N., & Ghafarian, P., (2016), *Investigation of meteorological parameters in the lower and upper troposphere during tropical cyclone Haiyan*, Journal of Oceanography 726:55-67.
29- Pegahfar, N., & Ghafarian, P., (2017), *Dynamic and Thermodynamic Analysis of Tropical Cyclone Haiyan*, Journal of Space and Earth Physics, 424, 13-26.
30- Pielke, Jr. R., Gratz, J., Landsea, C., Collins, D., Saunders, M., & Musulin, R., (2008), *Normalized hurricane damages in the United States: 1900-2005*. Natural Hazards Rev., 9, 29–42.
31- Riehl, H., (1951), *A model for hurricane formation*, J. Appl. Phys., Vol. 21, 917–925.
32- Schenkel, B. A., Lin, N., Chavas, D., Vecchi, G. A., Oppenheimer, M., & Brammer, A., (2018), *Lifetime Evolution of Outer Tropical Cyclone Size and Structure as Diagnosed from Reanalysis and Climate Model Data*, Journal of Climate, 31(19), 7985-8004.
33- Shimada, U., Kubota, H., Yamada, H., Cayanan, E. O., & Hilario, F. D., (2018), *Intensity and Inner-Core Structure of Typhoon Haiyan (2013) near Landfall: Doppler Radar Analysis*, Monthly Weather Review, 146(2), 583-597.

34- Smith, R., Ulrich, W., & Sneddon, G., (2000), *On the dynamics of hurricane-like vortices in vertical-shear flows: Quart*, J. Roy. Meteor. Soc., 126, 2653–2670.

35- Tang, B., & Camargo, S. J., (2014), *Environmental control of tropical cyclones in CMIP5: A ventilation perspective*, Journal of Advances in Modeling Earth Systems, 61, 115-128.

36- Tang, B., & Emanuel, K., (2010), *Midlevel ventilation's constraint on tropical cyclone intensity*, J. Atmos. Sci., 67, 1817–1830.

37- Tang, B. H. A., (2010), *Midlevel ventilation's constraint on tropical cyclone intensity*, Doctoral Thesis, Massachusetts Institute of Technology.

38- Tory, K., Davidson, N., & Montgomery, M., (2007), *Prediction and diagnosis of tropical cyclone formation in an NWP system. Part III: Diagnosis of developing and nondeveloping storms*, J. Atmos. Sci., 64, 3195–3213.

39- Vickery, P.J., F.J. Masters, M.D. Powell and D. Wadhera, (2009), *Hurricane hazard modelling: the past, present and future*, Journal of Wind Engineering and Industrial Aerodynamics, 97, 392-405.

40- Wang, Y., (2012), *Recent research progress on tropical cyclone structure and intensity*, Trop. Cyclone Res. Rev, 1, 254-275.

41- Wang, G., Zhao, B., Qiao, F., & Zhao, C., (2018), *Rapid intensification of Super Typhoon Haiyan: the important role of a warm-core ocean eddy*, Ocean Dynamics, 68(12), 1649-1661.

42- Wong, M. & Chan, J., (2004), *Tropical cyclone intensity in vertical wind shear*, J. Atmos. Sci., 61, 1859–1876.

43- Zehr, R., (1992), *Tropical cyclogenesis in the western north Pacif ic*, NOAA Tech. Rep. NESDIS 61, 181 pp.